Mon. Not. R. Astron. Soc. **343,** 1181–1194 (2003)

An *XMM–Newton* hard X-ray survey of ultraluminous infrared galaxies

A. Franceschini,[1⋆] V. Braito,[1,2] M. Persic,[3] R. Della Ceca,[4] L. Bassani,[5] M. Cappi,[5] P. Malaguti,[5] G. G. C. Palumbo,[6] G. Risaliti,[7,8] M. Salvati[7] and P. Severgnini[4]

[1]*Dipartimento di Astronomia, Università di Padova, Vicolo Osservatorio 2, I-35122, Italy*
[2]*INAF-Osservatorio Astronomico di Padova, Vicolo Osservatorio 5, I-35122, Italy*
[3]*INAF-Osservatorio Astronomico di Trieste, via G. B. Tiepolo 11, 34131 Trieste, Italy*
[4]*INAF-Osservatorio Astronomico di Brera, via Brera, 28, I-20121 Milano, Italy*
[5]*IASF-CNR, Sezione di Bologna, via Gobetti 101, 40129 Bologna, Italy*
[6]*Dipartimento di Astronomia, Università di Bologna, via Ranzani 1, 40127 Bologna, Italy*
[7]*INAF-Osservatorio Astrofisico di Arcetri, Largo E. Fermi 5, 50125 Firenze, Italy*
[8]*Harvard-Smithsonian Center for Astrophysics, 60 Garden Street Cambridge, MA 02138, USA*

Accepted 2003 April 26. Received 2003 April 17; in original form 2002 November 20

ABSTRACT

XMM–Newton observations of 10 ultraluminous infrared galaxies (ULIRGs) from a 200-ks mini-survey programme are reported. The aim is to investigate in hard X-rays a complete ULIRG sample selected from the bright *IRAS* 60-μm catalogue. All sources are detected in X-rays, five of which for the first time. These observations confirm that ULIRGs are intrinsically faint X-ray sources, their observed X-ray luminosities being typically $L_{2-10\,\mathrm{keV}} \leqslant 10^{42}$–$10^{43}$ erg s^{-1}, whereas their bolometric (mostly infrared) luminosities are $L_{\mathrm{bol}} > 10^{45}$ erg s^{-1}. In all sources we find evidence for thermal emission from hot plasma with a rather constant temperature $kT \simeq 0.7$ keV, dominating the X-ray spectra below 1 keV, and probably associated with a nuclear or circumnuclear starburst. This thermal emission appears uncorrelated with the far-infrared luminosity, suggesting that, in addition to the ongoing rate of star formation, other parameters may also affect it. The soft X-ray emission appears to be extended on a scale of ∼30 kpc for Mrk 231 and IRAS 19254−7245, possible evidence of galactic superwinds. In these two sources, IRAS 20551−4250 and 23128−5919, we find evidence for the presence of hidden active galactic nuclei (AGNs), while a minor AGN contribution may be suspected also in IRAS 20100−4156. In particular, we have detected a strong (EW ∼ 2 keV) Fe K line at 6.4 keV in the spectrum of IRAS 19254−7245 and a weaker one in Mrk 231, suggestive of deeply buried AGNs. For the other sources, the X-ray luminosities and spectral shapes are consistent with hot thermal plasma and X-ray binary emissions of mainly starburst origin. We find that the 2–10 keV luminosities in these sources, most probably due to high-mass X-ray binaries, are correlated with L_{FIR}: both luminosities are good indicators of the current global star formation rate in the Galaxy. The composite nature of ULIRGs is then confirmed, with hints for a predominance of the starburst over the AGN phenomenon in these objects even when observed in hard X-rays.

Key words: surveys – galaxies: active – galaxies: evolution – galaxies: starburst – infrared: galaxies – X-rays: galaxies.

1 INTRODUCTION

Ultraluminous infrared galaxies (ULIRGs, sources with bolometric luminosity $L_{\mathrm{IR}} > 10^{12}\ \mathrm{L}_{\odot}$ mostly emitted in the infrared) have received much attention since their discovery during the *IRAS* survey follow-up observations (Sanders et al. 1988; see a review in Sanders & Mirabel 1996). The main reason for this interest was that, together with optical quasars, these are by far the most luminous objects in the Local Universe.

The relevance of this class of sources in the cosmological context has been further emphasized by recent findings of cosmological surveys at long wavelengths. Observations at infrared (IR) and submillimetre wavelengths have discovered that luminous and ultraluminous IR galaxies, which are rare in the Local Universe (Soifer

⋆E-mail: franceschini@pd.astro.it

et al. 1987), are detected instead in large numbers in deep-IR surveys, and are a fundamental constituent of the high-redshift galaxy population (e.g. Smail, Ivison & Blain 1997; Genzel & Cesarsky 2000; Franceschini et al. 2001). The number and luminosities of these sources imply that an important fraction of stars in present-day galaxies, or alternatively of the degenerate baryons contained in nuclear supermassive black holes, have formed during such IR-luminous dust-extinguished evolutionary phases in the past. It has been argued that luminous and ultraluminous IR galaxies at high redshifts could trace events of star formation that may be at the origin of massive elliptical and S0 galaxies (e.g. Franceschini et al. 1994; Lilly et al. 1999). Support for this view has recently come from high-resolution spectroscopy of ULIRG mergers (Genzel & Cesarsky 2001), whose dynamical properties have proven that they indeed are 'ellipticals in formation'.

This evidence came along with the discovery by *COBE* of a bright diffuse radiation, the cosmic IR background (CIRB, see Hauser et al. 1998; Lagache et al. 2000), apparently containing a large fraction (up to ~70 per cent) of the total extragalactic background energy density from radio to X-rays, i.e. a major part of the photon energy released by cosmic sources at any redshift. As discussed by various authors (Elbaz et al. 2002; Smail et al. 2002), there is precise evidence that this background radiation is indeed produced by sources similar in all respects to luminous and ultraluminous IR galaxies at $z \geqslant 0.5$. These recent facts justify the growing interest in local ULIRGs as possible clues to their supposed high-z counterparts.

However, about 15 yr after their discovery, the nature of these sources still remains rather enigmatic. Large gas and dust column densities in the galaxy cores, responsible for the IR emission, prevent a direct observation of the primary energy source, and the IR spectral shapes are highly degenerate with respect to the illuminating spectrum. It is widely accepted that both starburst and active galactic nucleus (AGN) activity may be responsible for the observed luminosities (Genzel et al. 1998; Veilleux, Kim & Sanders 1999; Risaliti et al. 2000; Bassani et al., in preparation). If indeed ULIRGs are 'forming spheroids', an AGN/starburst association is naturally supported by the evidence that all spheroidal galaxies host quasar relics in the form of supermassive black holes. The same radial inflow of gas produced by the merger is likely to fuel both the starburst and, at some stages, the AGN.

So far conflicting evidence has been reported about the relative contributions of the two energy sources in ULIRGs, stellar and gravitational. Important progress has been achieved with mid- and far-infrared (mid-, far-IR) spectroscopy, probing the inner optically thick nuclei. Using diagnostics based on coronal line intensities and polycyclic aromatic hydrocarbon (PAH) line-to-continuum ratios, Lutz et al. (1996), Genzel et al. (1998) and Rigopoulou et al. (1999) have argued that the majority of ULIRGs are powered by star formation.

On the other hand, the presence of energetically important obscured AGNs in ULIRGs has been revealed by optical and near-infrared (near-IR) spectroscopy, often detecting Seyfert-like nuclear emission-line spectra (Sanders et al. 1988; Veilleux, Sanders & Kim 1997) as well as evidence for completely buried AGNs (Soifer et al. 2001; Imanishi, Dudley & Maloney 2001).

In principle, hard X-ray observations offer an additional important tool to investigate the presence of hidden AGNs, providing quantitative estimates of their contribution to the bolometric luminosity. This diagnostic relies on the fundamentally different spectra and luminosity regimes between starbursts and AGNs in hard X-rays. Hard continuum emission and prominent Fe Kα line(s) are distinguishing features of buried AGNs, which can penetrate large gas column densities. Some of the brightest nearby ULIRGs, classified on the basis of IR spectroscopy as pure starburst, show spectral properties typical of obscured AGNs when observed in hard X-rays (e.g. NGC 6240, Iwasawa 1999; Vignati et al. 1999). In practice, so far the utilization of this diagnostic has been limited by the X-ray faintness of most ULIRGs [see previous unsuccessful detection attempts with *ROSAT*, *ASCA* and *BeppoSAX* (Risaliti et al. 2000)].

The unique large collective area and hard X-ray response of *XMM–Newton* have been used here to deeply survey for the first time a representative sample of 10 *IRAS*-selected ULIRGs for which high-quality mid-IR and optical spectroscopy data are available. Most of these ULIRGs were previously classified as starbursts (Lutz, Veilleux & Genzel 1999). The purpose of the present observations is not only to identify AGN signatures in hard X-rays, but also to quantify separately the contributions of the buried AGN from the starburst emission to the X-ray spectra, and to compare them with independent estimates based on optical and IR observations. This paper summarizes the main X-ray properties of the sample, five sources of which are detected in X-rays for the first time. *XMM–Newton* observations for two sources of the sample of particular interest, the Superantennae and Mrk 231, are discussed in separate papers (Braito et al. 2003a,b).

Section 2 summarizes the properties of our ULIRG sample. Section 3 details the *XMM–Newton* observations and data analysis. The resulting hard X-ray properties are reported in Section 4, while Section 5 discusses plausible origins of various X-ray components and compares them with data at other wavelengths. Section 6 contains our conclusions. $H_0 = 50$ km s^{-1}Mpc^{-1} has been assumed throughout.

2 THE ULIRG SAMPLE

The sample of 10 ULIRGs discussed in this paper has been selected from the list of *IRAS* ULIRGs observed with *ISO* by Genzel et al. (1998). The sample is flux-limited at 60 μm and complete to $S_{60\,\mu m} \geqslant 5.4$ Jy. It includes sources with $L \geqslant 10^{12}$ L$_\odot$ in the total 8–1000 μm band, whose far-IR selection makes it unbiased with respect to absorption and representative of the most luminous galaxies in the Local Universe. High-quality IR/optical spectroscopic data are available for all the sample sources (Lutz et al. 1999; Veilleux et al. 1999).

Of the original Genzel et al. (1998) sample of 15 ULIRGs, four have been observed with *XMM–Newton* by different teams, while IRAS 23060+0505 has been deeply observed with *ASCA* (Brandt et al. 1997) and *BeppoSAX*. Source names, sky positions (which are also the coordinates of the *XMM* EPIC observations), IR (8–1000 μm) luminosities, redshifts, as well as the *XMM* EPIC net exposure times and observation dates, of the 10 ULIRGs presented here, are reported in Table 1. Optical and IR classifications of the ULIRGs presented here will be summarized in Table 4.

All 10 objects have been observed with *XMM–Newton* with ~20-ks exposure each. A fraction of the observations had to be excluded from the analysis because of background flares (this problem was severe for the source IRAS 23128−5919, see Table 1).

3 *XMM–NEWTON* EPIC DATA PREPARATION AND ANALYSIS

The *XMM–Newton* observations presented here have been performed between 2001 March and 2002 November with the EPIC (European Photon Imaging Camera: Strüder et al. 2001; Turner et al.

Table 1. The source sample and summary of the *XMM–Newton* observations.

Name	Coordinates (J2000)	z	$L_{\rm IR}$ (10^{12} L$_\odot$)	PN net exp. time (ks)	Obs. date	Sequence	Filter
IRAS 12112+0305	12 13 46.03 +02 48 41.5	0.072	3.8	20.9	2001 Dec 30	0081340801	Medium(PN)–thin
Mrk 231[a]	12 56 14.16 +56 52 24.9	0.042	6.7	19.8	2001 Jun 06	0081340201	Medium
IRAS 14348−1447	14 37 38.30 −15 00 23.0	0.082	4.0	17.5	2002 Jul 29	0081341401	Medium
IRAS 15250+3609	15 26 59.43 +35 58 37.4	0.055	2.0	17.8	2002 Feb 22	0081341101	Thin
IRAS 17208−0014	17 23 22.03 −00 17 00.3	0.043	4.7	15.7	2002 Feb 19	0081340601	Medium
IRAS 19254−7245[b]	19 31 21.46 −72 39 21.6	0.062	2.2	18.4	2001 Mar 21	0081341001	Thin
IRAS 20100−4156	20 13 29.75 −41 47 34.0	0.129	7.4	18.1	2001 Apr 21	0081340501	Medium
IRAS 20551−4250	20 58 27.05 −42 39 06.8	0.043	2.1	16.1	2001 Apr 21	0081340401	Thin
IRAS 22491−1808	22 51 49.26 −17 52 24.0	0.078	2.7	21.7	2001 May 24	0081340901	Medium
IRAS 23128−5919	23 15 47.00 −59 03 17.0	0.044	2.0	9.4	2002 Nov 19	0081340301	Medium

Notes. [a]*XMM–Newton* observations reported in Braito et al. (2003b). [b]*XMM–Newton* observations reported in Braito et al. (2003a).

2001) cameras operating in full-frame mode. Data have been processed using the Science Analysis Software (SAS version 5.4), and have been analysed using standard software packages (FTOOLS 5.0, XSPEC 11.0). The latest calibration files released by the EPIC team have been used.

Event files produced from the pipeline have been filtered from high-background time intervals, and only events corresponding to pattern 0-12 for MOS and pattern 0-4 for PN have been used (see the *XMM–Newton* Users' Handbook, Ehle et al. 2001). We have then generated our own response matrices (that include the correction for the effective area) using the SAS tasks ARFGEN and RMFGEN. The screening process from high-background time intervals yielded net exposures between 15.7 and 21.7 ks (net exposures for PN camera are reported in Table 1), with the exception of IRAS 23128−5919 (9.4 ks).

All the 10 ULIRGs have been detected in the MOS1, MOS2 and PN detectors with signal-to-noise ratios S/N > 3. Close-up images of the sources are reported in Figs 1–3 as overlays of the (0.2–10 keV) X-ray contours on top of the POSS red-band images. For all the ULIRGs the bulk of the X-ray emission is positionally coincident (within the *XMM–Newton* positional error) with the optical–IR core. By accounting in detail for the EPIC point spread function (PSF), we have found evidence for extended emission only in Mrk 231 and IRAS19254−7245, while the surface brightness distributions for all other sources are consistent with being unresolved by EPIC.

Except for Mrk 231, the most extended source (90 per cent counts in ∼40 arcsec in the soft X-ray band $E < 2$ keV), the source spectra were extracted from circular regions of ∼20 arcsec radius. Background spectra have been extracted from source-free circular regions (with typically ∼1 arcmin radius) close to the target.

In order to improve the statistics, MOS1 and MOS2 data have been combined. Both MOS and PN spectra were then automatically rebinned in order to have $\geqslant$20 counts in each energy channel. The combined MOS data have been fitted simultaneously with the PN data, by keeping the relative normalizations free.

4 RESULTS

We report in Table 2 the measured fluxes and luminosities of the sources in various X-ray bands. Our *XMM–Newton* observations show that ULIRGs are rather faint in X-rays if compared with AGNs of similar bolometric (IR) luminosities. Their observed X-ray luminosities are close to or lower than $L_{2-10\,\rm keV} = 10^{42}$ erg s^{-1}, while their IR bolometric output is always $L_{\rm bol} > 10^{45}$ erg s^{-1}.

The level of detail for our spectral analysis is different for each source depending on the qualities of the *XMM* spectra, ranging from fairly detailed for stronger sources to only rather coarse spectral fits for the faintest. The two brightest sources, IRAS 19254−7245 and Mrk 231, have data of sufficiently high quality to guarantee investigations of both the continuum emission and the Fe K 6.4 keV line, detected only in these two sources (see Braito et al. 2003a,b).

At energies above 1 keV, the X-ray spectra appear to be dominated by a relatively flat power-law (PL) component in most of the sources. We tried to fit these overall 0.2–10 keV spectra with single-component models, either purely thermal or absorbed PL, as a zeroth-order attempt. For all sources, these simple fits were rejected with high statistical significance.

The *XMM–Newton* spectral data are shown in Figs 4 and 5 and compared with model spectra. The bottom panel in each figure displays the ratio of the observed to predicted flux as a function of energy. No emission lines are evident in these spectra, if we exclude Mrk 231 and IRAS 19254−7245. The only appreciable feature is a fairly sharp, well-characterized peak at $E \sim 0.7$–1 keV, likely to be of thermal origin. We have modelled this component with a thermal emission template using the routine MEKAL in XSPEC (Mewe, Gronenschild & van den Oord 1985), whose free parameters are the temperature kT and the normalization. The plasma metallicity has been set, for simplicity, to the solar value. This has no effect on our estimate of the plasma temperature, the assumed metallicity essentially affecting only the normalization of the thermal spectrum.

In the rest of the present section we discuss each source separately. The best-fitting parameters are summarized in Table 3. More detailed spectral decompositions are discussed in Section 5.

4.1 IRAS 19254–7245, the Superantennae

From the analysis of the *ASCA* data (Imanishi & Ueno 1999; Pappa, Georgantopoulos & Stewart 2000), two alternative fits were proposed for this object: (a) unabsorbed PL model with flat photon index ($\Gamma \sim 1$), and (b) absorbed PL model with $\Gamma \simeq 1.8$ and $N_{\rm H} \sim 10^{22}$ cm^{-2}. No Fe K lines were detected by *ASCA*.

XMM–Newton has detected a strong X-ray flux from IRAS 19254−7245. As shown in Fig. 1, the emission is centred in the southern nucleus of the interacting pair, while no hard X-ray emission is apparently related to the northern one. This is consistent with the results from observations at other wavelengths, which show that the southern nucleus, classified as a type 2 Seyfert galaxy, is always brighter than the northern one (Melnick & Mirabel 1990). By taking into account the EPIC PSF, the X-ray source appears to be

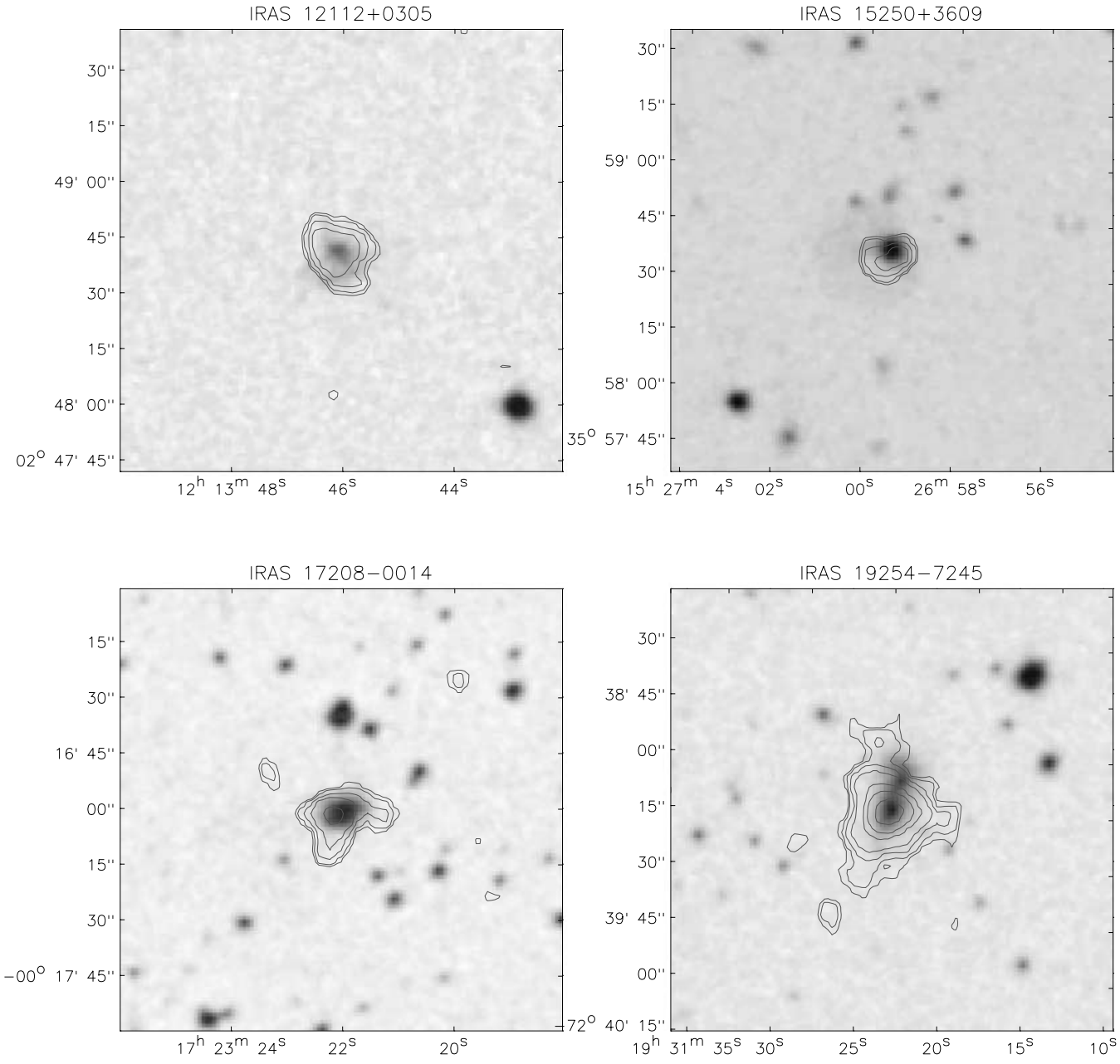

Figure 1. DSS2 images (2×2 arcmin^2) of IRAS 12112+0305, 15250+3609, 17208−0014 and 19254−7245 (from top left to bottom right). Contours of the X-ray (0.2–10 keV) emission have been overlaid. The contours displayed correspond to 4σ, 5σ, 7σ, 10σ, 20σ, 30σ, 50σ above the background. The contours have been derived using the MOS2 data, since this detector has the best point spread function (see Ehle et al. 2001).

significantly extended at low energies ($E < 2$ keV). A detailed analysis of this complex source, resembling in many aspects the prototypical type II quasar NGC 6240, is reported in Braito et al. (2003a).

A single unabsorbed PL model is not a good description of the *XMM–Newton* data because it seriously misfits the spectrum at low energies. By adding a thermal component to their composite model, Braito et al. (2003a) have obtained a temperature $kT = 0.85^{+0.1}_{-0.1}$ keV for the thermal component and $\Gamma = 1.84 \pm 0.20$ ($N_{\rm H} = 4.7 \times 10^{21}$ cm^{-2}) for the hard PL component. The soft X-ray luminosity is $\sim$1.8 $\times\ 10^{42}$ erg s^{-1}. Braito et al. (2003a) have also found evidence for a Fe K line at 6.4 keV, whose large equivalent width (EW $\simeq$ 1.4 keV), together with the flat photon index, indicates that this object is a 'Compton-thick' AGN, in which the detected hard X-ray emission is due to a pure reflected component plus a scattered one. Hence, the intrinsic AGN luminosity is much higher than the observed value of $\sim 10^{42}$ erg s^{-1}, and probably $\geqslant 10^{44}$ erg s^{-1}.

4.2 Mrk 231

Among local ULIRGs, Mrk 231 is the most luminous object in the IR (Soifer et al. 1984) and one of the best studied at all wavelengths. Observed with many X-ray instruments (*ROSAT*, *ASCA* and *Chandra*), its X-ray properties still remain puzzling. Evidence of a combined AGN and starburst activity emerged from the *ROSAT* and *ASCA* data (Imanishi & Ueno 1999; Turner 1999). However,

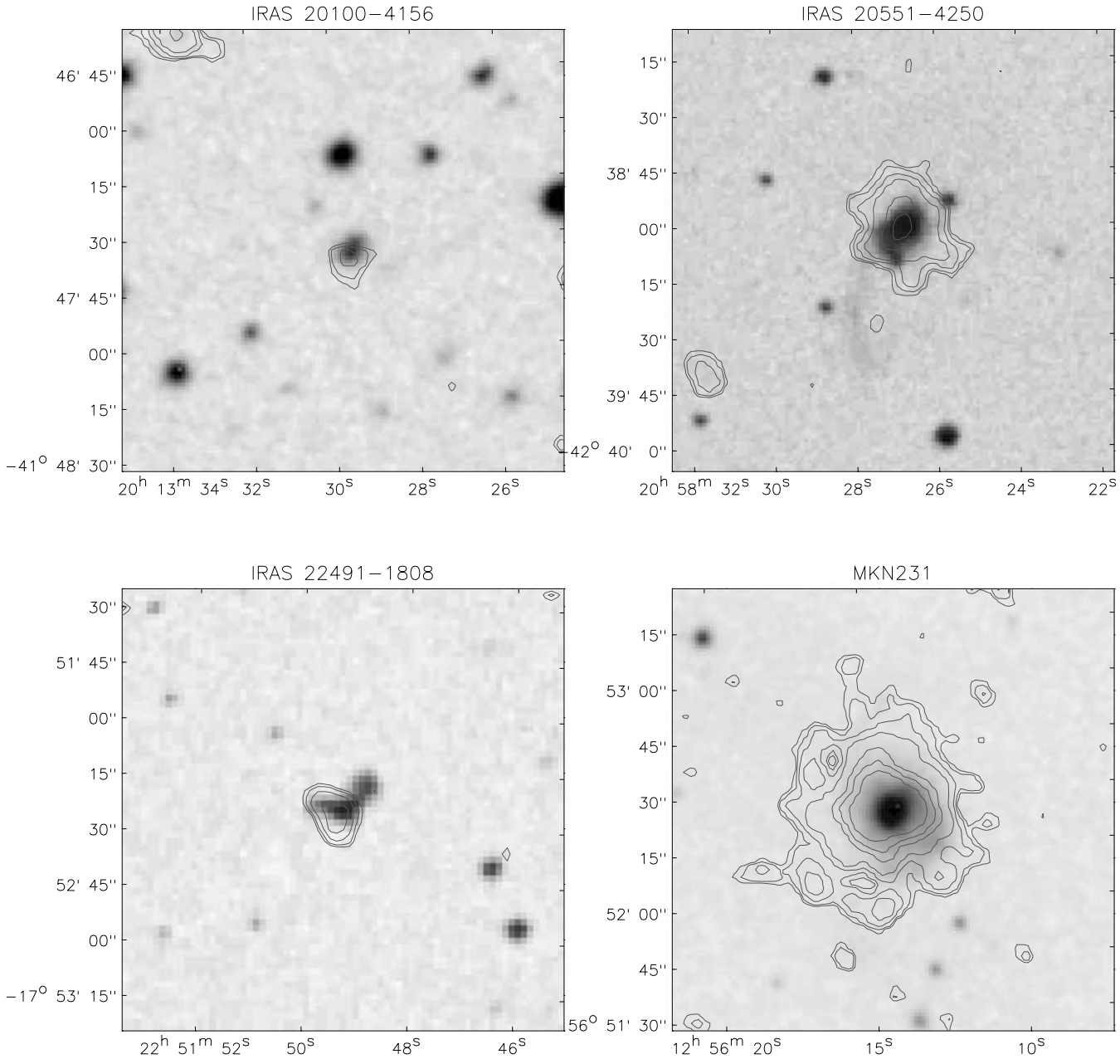

Figure 2. DSS2 images (2×2 arcmin^2) of IRAS 20100−4156, 20551−4250, 22491−1808 and Mrk 231 (from top left to bottom right). Contours of the X-ray (0.2–10 keV) emission have been overlaid. The contours displayed (from the MOS2 data) correspond to 4σ, 5σ, 7σ, 10σ, 20σ, 30σ, 50σ above the background. See also caption to Fig. 1.

the flatness of the X-ray spectrum at energies above 2 keV and the lack of detection of any strong Fe lines (Maloney & Reynolds 2000) appeared unusual. These results have been confirmed with a recent *Chandra* observation ($\Gamma = 1.3$, Fe K line with EW < 188 eV; see Gallagher et al. 2002).

Our *XMM–Newton* field containing the source is shown in Fig. 2: the source appears very bright and extended. This extension is significantly in excess of the PSF only for low-energy photons ($E < 2$ keV), with a total diameter of ∼1 arcmin (∼50 kpc), while for higher-energy photons the source spatial profile is consistent with the PSF. A detailed analysis of the *XMM–Newton* data on Mrk 231, plus those from a deep *BeppoSAX* observation extending up to 80 keV, is reported in a companion paper by Braito et al. (2003b). Our results also confirm the very flat spectrum and the detection of a moderately intense (EW ∼ 200 eV) Fe Kα line at 6.4 keV. The luminosity of the hard component is $\sim 3 \times 10^{42}$ erg s^{-1}. The presence of a highly obscured AGN is then confirmed by the *BeppoSAX* PDS data, but our *XMM–Newton* observations suggest the concomitant presence of an important starburst component.

4.3 IRAS 20551–4250 and 23128–5919

IRAS 20551−4250 has been previously detected with *ASCA* (Misaki et al. 1999), but at a very low significance level. *XMM–Newton*

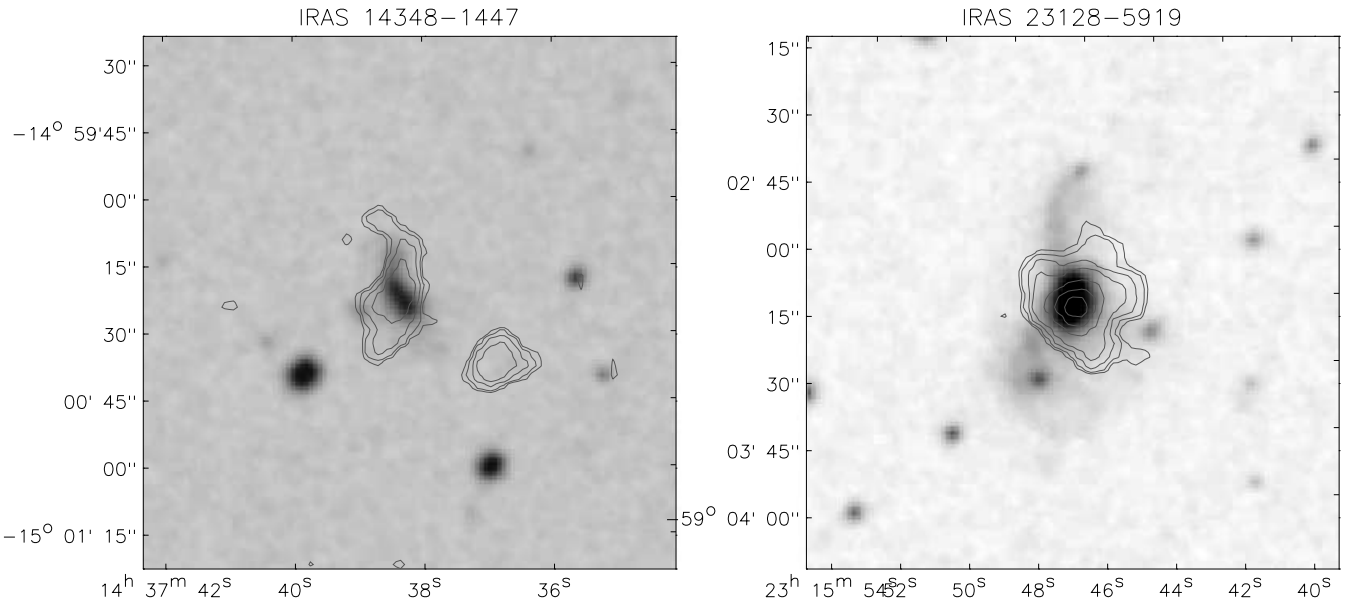

Figure 3. DSS2 images and *XMM–Newton* contours (2×2 arcmin^2) of IRAS 14348−1447 and 23128−5919. Contours of the X-ray (0.2–10 keV) emission have been overlaid. The contours displayed (from the MOS2 data) correspond to 4σ, 5σ, 7σ, 10σ, 20σ, 30σ, 50σ above the background. See also caption to Fig. 1.

Table 2. Source fluxes and luminosities.

Name	Counts[a] PN+MOS1+MOS2	$S_{0.5-2\,\mathrm{keV}}$[b] (erg cm^{-2}s^{-1})	$S_{2-10\,\mathrm{keV}}$[b] (erg cm^{-2} s^{-1})	$L_{0.5-2\,\mathrm{keV}}$[c] (erg s^{-1})	$L_{2-10\,\mathrm{keV}}$[c] (erg s^{-1})
IRAS 12112+0305	256 ± 21	1.2×10^{-14}	1.5×10^{-14}	3.4×10^{41}	3.6×10^{41}
Mrk 231	2535 ± 51	1.1×10^{-13}	6.5×10^{-13}	2.2×10^{42}	6.4×10^{42}
IRAS 14348−1447	297 ± 24	1.8×10^{-14}	2.0×10^{-14}	8.9×10^{41}	5.5×10^{41}
IRAS 15250+3609	433 ± 26	2.1×10^{-14}	2.4×10^{-14}	3.0×10^{41}	3.0×10^{41}
IRAS 17208−0014	401 ± 31	2.3×10^{-14}	4.0×10^{-14}	6.0×10^{41}	3.6×10^{41}
IRAS 19254−7245	926 ± 33	5.3×10^{-14}	2.3×10^{-13}	1.8×10^{42}	2.9×10^{42}
IRAS 20100−4156	101 ± 17	5.4×10^{-15}	1.9×10^{-14}	1.2×10^{42}	1.6×10^{42}
IRAS 20551−4250	942 ± 39	5.5×10^{-14}	1.4×10^{-13}	4.2×10^{42}	7.9×10^{42}
IRAS 22491−1808	232 ± 19	1.0×10^{-14}	6.4×10^{-15}	1.6×10^{41}	1.7×10^{41}
IRAS 23128−5919	833 ± 34	4.95×10^{-14}	1.7×10^{-13}	1.0×10^{42}	1.8×10^{42}

Notes. [a]Total net counts used in the spectral fits. [b]Observed fluxes. [c]Luminosities are corrected for Galactic and intrinsic (N_H) absorption.

detects it with a high enough S/N ratio to allow us to perform a detailed spectral analysis. The source appears as unresolved by EPIC (see Fig. 2).

A good fit (Fig. 5) is obtained only with a three-component model: a thermal model ($kT = 0.68^{+0.12}_{-0.07}$ keV), and a 'leaky-absorber' continuum, including an absorbed plus a non-absorbed power-law spectrum with the same photon index. We found that a good fit can be obtained with $\Gamma = 1.8^{+0.2}_{-0.2}$ and $N_\mathrm{H} = 8 \times 10^{23}$ cm^{-2}. The 6.4 keV Fe K line is not detected, but the upper limit on its equivalent width ($\leqslant$1 keV) is consistent with the N_H value obtained from the fit. The intrinsic 2–10 keV luminosity of this object, corrected for absorption, is $\sim 7.0 \times 10^{42}$ erg s^{-1}, while the soft X-ray luminosity is $\sim 4.2 \times 10^{42}$ erg s^{-1}. The high X-ray luminosity and the properties of the X-ray spectrum clearly suggest the presence of an extinguished AGN.

The *XMM–Newton* observations of IRAS 23128−5919 have been strongly affected by high background (only 9.4 ks of good data are available), and this prevented us from attempting detailed spectral fits. The source appears as point-like and relatively luminous. The spectrum is reasonably well reproduced by the sum of a thermal model and a simple power law with no absorption. However, the power law's spectral index in this solution is unphysically hard ($\Gamma = 1.04 \pm 0.13$), suggesting the presence of an absorbed component. We then adopted the same 'leaky-absorber' model as discussed for IRAS 20551−4250, and found best-fitting parameters $kT = 0.65 \pm 0.15$ keV, $\Gamma = 1.67^{+0.09}_{-0.34}$ and $N_\mathrm{H} = 6.9 \pm 3.5 \times 10^{22}$ cm^{-2}. The luminosities of the thermal and de-absorbed power-law components are $\sim 1.5 \times 10^{41}$ and $\sim 2.7 \times 10^{42}$ erg s^{-1}. The large gas column density and power-law luminosity clearly indicate the presence of an AGN, whereas a spectroscopic IR study by Charmandaris et al. (2002) revealed the predominance of a starburst. Our subsequent analysis in Section 5.3 suggests that IRAS 23128−5919 is a transition object, with properties intermediate between those of an AGN and a starburst.

4.4 IRAS 14348–1447, 15250+3609 and 17208–0014

All these sources have intermediate-quality detections. While the latter two are consistent with a point-source emission at all energies, IRAS 14348−1447 appears to be resolved in a bow-like structure

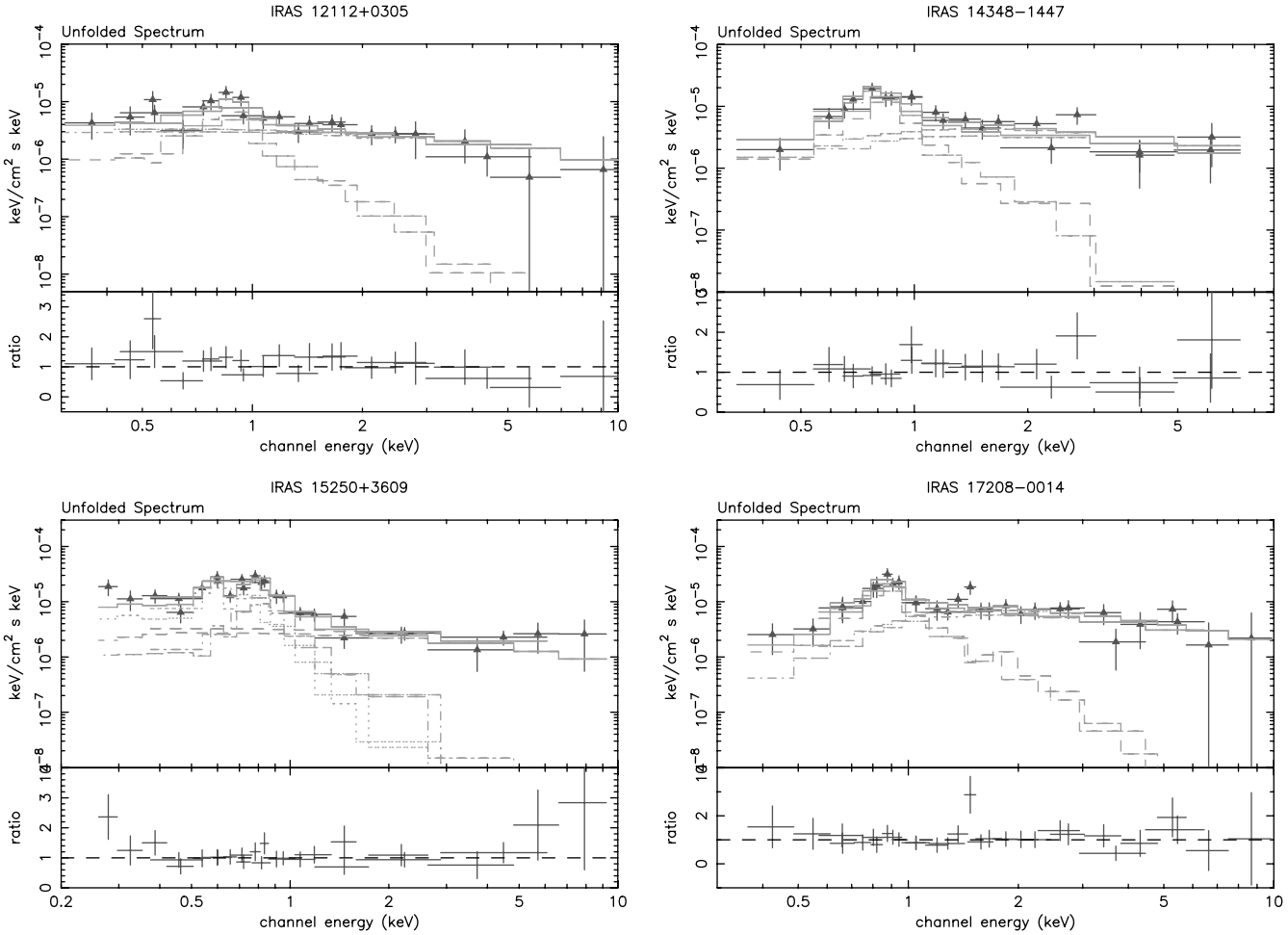

Figure 4. *XMM–Newton* spectra in energy units and ratios of data to the best-fitting model values as a function of energy, for the sources IRAS 12112+0305, 14348−1447, 15250+3609 and 17208−0014, from top left to bottom right.

of total size ∼30 arcsec in the north–south direction. The close-up image in Fig. 3 shows also the presence of another relatively bright ($S_{2-10\,\mathrm{keV}} \sim 5 \times 10^{-15}$ erg cm^{-2} s^{-1}) source located only 20 arcsec away in the south-east direction, a position in which no optical counterpart is detectable in the POSS image.

IRAS 14348−1447 and 17208−0014 show evidence of a single-temperature plasma emission with $kT \simeq 0.62 \pm 0.08$ keV and $kT \simeq 0.75 \pm 0.08$ keV, respectively. The spectrum of IRAS 15250+3609, instead, is unique among those from our spectral survey in requiring the presence of multitemperature plasmas (a two-temperature solution indicates $kT \simeq 0.26 \pm 0.09$ keV and $kT \simeq 0.64 \pm 0.15$ keV).

In addition to these thermal emissions, we find a very significant hard X-ray component in all three sources. Acceptable spectral fits have then been obtained by combining a Mekal-modelled thermal emission and an absorbed PL having $\Gamma \sim 2.2$, except for IRAS 15250+3609, whose photon index is flatter ($\Gamma \sim 1.2$) (see Table 4). In all sources some absorption in excess of the Galactic value is required ($N_{\mathrm{H}} > 10^{21}$ cm^{-2}). All three sources have X-ray luminosities in the range 10^{41}–10^{42} erg s^{-1}.

4.5 IRAS 12112+0305, 20100–4156 and 22491–1808

All these sources are detected at the lowest level of significance. This has prevented us from performing any detailed spectral analyses. On these sources we only tried two separate fits with a thermal model and an absorbed PL. For all three sources, a single thermal or a PL model are rejected by the data. Successful spectral fits require a combination of thermal and PL emissions (see Table 4).

The intrinsic hard (2–10 keV) X-ray luminosities are 1.7×10^{41} erg s^{-1} for IRAS 22491−1808, $\sim 1.6 \times 10^{42}$ erg s^{-1} for IRAS 20100−4156, and 3.6×10^{41} erg s^{-1} for IRAS 12112+0305.

5 THE SPECTRAL ANALYSIS

The X-ray spectral properties of the ULIRG sample appear to be fairly uniform. The spectra are well reproduced by the combination of soft thermal and hard PL components. For a physical interpretation of the ULIRG phenomenon, the implications of these results are briefly discussed in this and the next section. A more detailed comparison of these *XMM–Newton* spectra with model predictions is deferred to Persic et al. (in preparation).

5.1 Evidence for AGN-dominated emission

One of the motivations for the present survey has been the opportunity offered by hard X-ray data to constrain the relative AGN and starburst contributions to the source activity. A dominant AGN contribution should be detectable in X-rays as (a) a high-luminosity X-ray emission, $L_{2-10\,\mathrm{keV}} > 10^{42}$ erg s^{-1}, (b) highly extinguished hard X-ray components with $N_{\mathrm{H}} > 10^{22}$ cm^{-2}, as revealed by

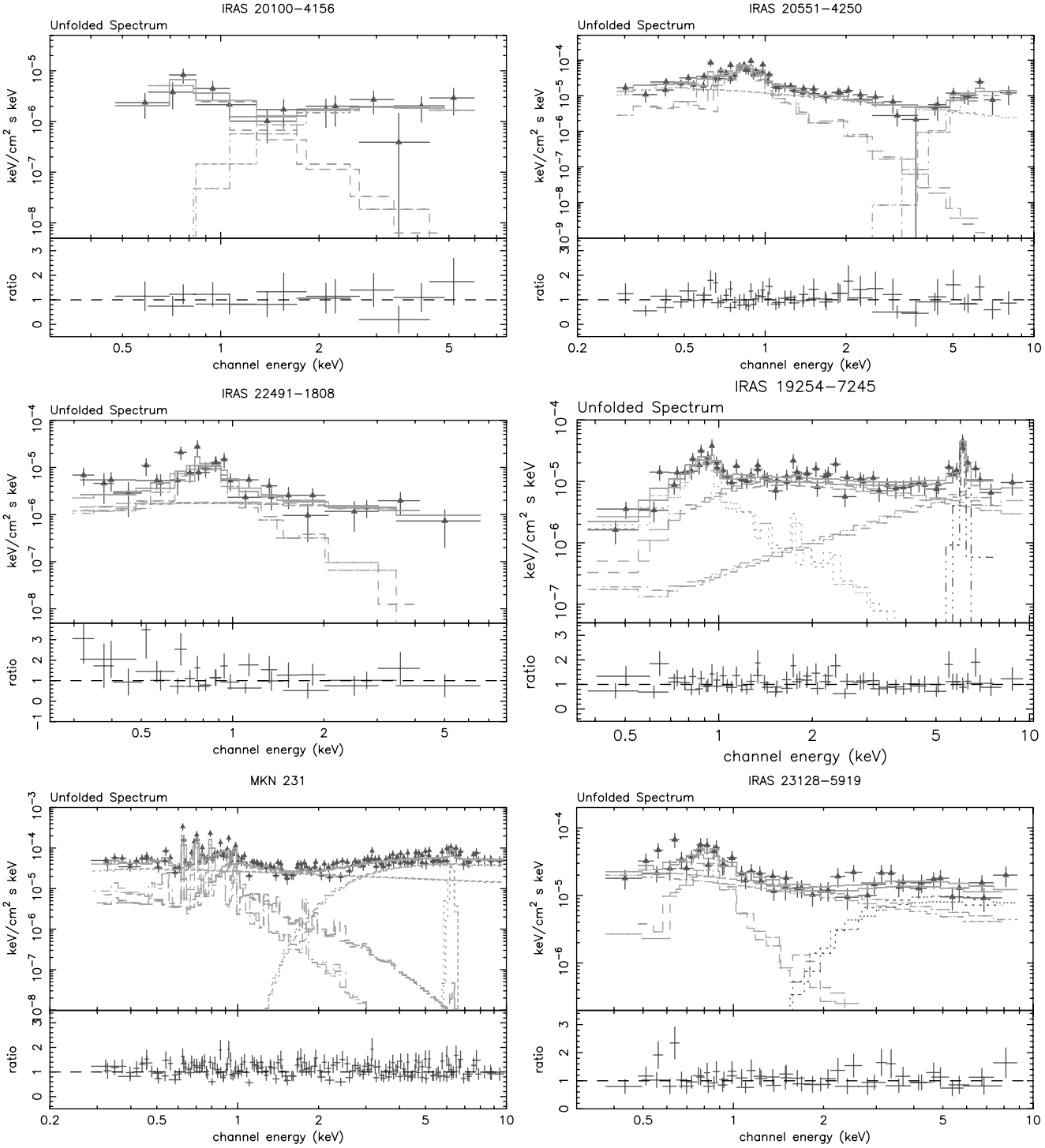

Figure 5. *XMM–Newton* spectra in physical units and ratios of data to the best-fitting model, for the sources IRAS 20100−4156, 20551−4250, 22491−1808, 19254−7245, Mrk 231 and IRAS 23128−5919.

very flat or inverted hard X-ray spectra, or (c) Fe K complexes at ∼6.4 keV with large equivalent widths (EW ∼ 1 keV), corresponding to iron fluorescent emission by cold molecular material illuminated by the energetic radiation field of the AGN.

We found such evidence for an AGN spectrum in four out of the 10 sources observed. The most obvious AGN is IRAS 19254−7245, which has both a strong Fe K line and a very flat (probably scattered) hard continuum, implying an intrinsic luminosity $L_{2-10\,\mathrm{keV}} > 10^{44}$ erg s^{-1} (Braito et al. 2003a).

The ULIRG Mrk 231 has been clearly identified from optical/IR observations as an AGN-dominated source, as inferred in particular from the flat, almost power-law, mid-IR continuum observed by Genzel et al. (1998) and the low EW of the PAH emissions. The source is also classified as a broad absorption-line quasar from

Table 3. Best-fitting spectral parameters.

Name	Model[c]	χ^2/ν	kT (keV)	$L_{\rm thermal}$ [d] (erg s^{-1})	Γ	$N_{\rm H}$ (cm^{-2})	$L_{\rm PL}$ [d] $L_{\rm binaries}$ [d] (erg s^{-1})
IRAS 12112+0305	A	14.9/17	$0.79^{+0.43}_{-0.25}$	0.8×10^{41}	$1.92^{+0.33}_{-0.55}$	$0.8^{+1.4}_{-0.8} \times 10^{21}$	6.3×10^{41}
	B	16.3/18	$0.80^{+0.24}_{-0.16}$	1.1×10^{41}	1.1*	–	6.1×10^{41}
Mrk 231[a]	D[f]	196.8/156	$0.96^{+0.09}_{-0.14}$ $0.37^{+0.09}_{-0.05}$	3.7×10^{41}	$1.30^{+0.16}_{-0.15}$	$7.39^{+0.19}_{-0.91} \times 10^{21}$	8.3×10^{42}
IRAS 14348−1447	A	10.3/15	$0.61^{+0.20}_{-0.19}$	3.5×10^{41}	$2.18^{+0.51}_{-0.60}$	$0.3^{+0.7}_{-0.3} \times 10^{22}$	1.3×10^{42}
	B	13.7/16	$0.64^{+0.16}_{-0.13}$	3.7×10^{41}	1.1*	$0.5^{+2.6}_{-0.5} \times 10^{21}$	1.1×10^{42}
IRAS 15250+3609[b]	A	13.9/18	$0.64^{+0.14}_{-0.20}$ $0.26^{+0.08}_{-0.07}$	2.3×10^{41}	$1.21^{+0.62}_{-0.66}$	–	3.9×10^{41}
	B	14.9/18	$0.66^{+0.17}_{-0.10}$ $0.26^{+0.07}_{-0.07}$	2.2×10^{41}	1.1*	–	3.2×10^{41}
IRAS 17208−0014	A	16.3/24	$0.76^{+0.11}_{-0.12}$	1.6×10^{41}	$2.26^{+1.19}_{-0.98}$	$1.1^{+1.4}_{-1.1} \times 10^{22}$	8.1×10^{41}
	B	17.1/24	$0.74^{+0.14}_{-0.11}$	1.3×10^{41}	$1.30^{+0.10}_{-0.60}$	$2.6^{+7.2}_{-2.6} \times 10^{21}$	5.3×10^{41}
IRAS 19254−7245[a]	C	48.1/56	$0.85^{+0.14}_{-0.09}$	4.5×10^{41}	$1.84^{+0.60}_{-0.55}$	$0.47^{+0.52}_{-0.25} \times 10^{22}$	5.2×10^{42}
IRAS 20100−4156	A	4.8/8	$0.75^{+0.24}_{-0.32}$	4.1×10^{41}	1.7*	$2.6^{+4.9}_{-2.6} \times 10^{22}$	2.3×10^{42}
	B	4.7/8	$0.75^{+0.23}_{-0.26}$	4.1×10^{41}	1.1*	$2.2^{+4.8}_{-2.2} \times 10^{22}$	2.0×10^{42}
IRAS 20551−4250	E[f]	45.7/49	$0.66^{+0.10}_{-0.06}$	3.0×10^{41}	$1.8^{+0.20}_{-0.19}$	$7.9^{+6.9}_{-1.9} \times 10^{23}$	7.0×10^{42}
IRAS 22491−1808	A	22.9/21	$0.69^{+0.19}_{-0.21}$	1.5×10^{41}	$1.98^{+0.67}_{-0.63}$	–	3.6×10^{41}
	B	26.7/23	$0.66^{+0.15}_{-0.20}$	1.8×10^{41}	1.1*	–	3.8×10^{41}
IRAS 23128−5919	E[f]	32.7/44	$0.65^{+0.15}_{-0.14}$	1.5×10^{41}	$1.67^{+0.09}_{-0.34}$	$6.9^{+4.7}_{-3.4} \times 10^{22}$	2.7×10^{42}

Notes. [a]*XMM–Newton* observations reported in Braito et al. (2003a,b). [b]For this source an acceptable fit requires a two-temperature plasma. [c]Model A: thermal emission plus an absorbed power-law model; model B: thermal emission plus cut-off power law; model C: thermal emission plus a Compton reflected and scattered continuum (see Braito et al. 2003a); model D: two thermal emission plus a 'leaky absorber'; model E: thermal emission plus a 'leaky-absorber' continuum. [d]Luminosities are between 0.5 and 10 keV. [f]The covering factors for the 'leaky-absorber' continuum are 50, 95 and 54 per cent for Mrk 231, IRAS 20551−4250 and 23128−5919 respectively. NB: The symbol *indicates that the parameter has been kept fixed.

optical spectroscopy (Smith et al. 1995). The *XMM–Newton* observations reveal a moderate-luminosity X-ray source with a very flat spectrum ($\Gamma \simeq 0.9$) between 1 and 10 keV, while *BeppoSAX* data reported by Braito et al. (2003b) reveal a highly extinguished ($N_{\rm H} > 10^{24}$ cm^{-2}) component above 10 keV. These data fully confirm the classification of Mrk 231 as a dusty and extinguished AGN.

IRAS 20551−4250 is a third ULIRG with evidence from the *XMM–Newton* spectrum of harbouring a high column density ($N_{\rm H} \sim 10^{24}$ cm^{-2}) extinguished AGN, and similar evidence for the presence of a low-luminosity AGN was found in IRAS 23128−5919. Neither these two sources nor IRAS 19254−7245 showed evidence for AGN activity from IR spectroscopy (Genzel et al. 1998), which illustrates the useful complementarity between the IR and the X-ray approaches. A detailed spectrophotometric study of the Superantennae by Berta et al. (2003) has found evidence, however, for combined AGN and starburst emissions with comparable IR bolometric luminosities.

Further indications about the relative AGN/starburst contributions will come from the comparison of soft X-ray thermal and hard X-ray power-law emissions discussed in Section 5.3.

5.2 Starburst emission

The spectra of local starburst (SB) galaxies in the 0.5–10 keV band can be described as a combination of warm thermal emission (with typically $kT \simeq 0.6$–0.8 keV) dominating at energies $\leqslant$1 keV, plus a harder spectrum producing the bulk of the 2–10 keV flux. The warm thermal component is interpreted as originating from the boundary region between the hot, tenuous outgoing Galactic wind and the cool, dense interstellar medium (e.g. Strickland et al. 2000). The harder component has various interpretations in the literature,[1] either in terms of a very hot ($kT \geqslant 5$ keV) thermal or a $\Gamma \sim 2$ PL model, but no definitive conclusions were reached, as the thermal and PL fits are, in general, similarly successful.

Recently, Persic & Rephaeli (2002, see also David, Jones & Forman 1992) have developed a detailed quantitative model of synthetic X-ray spectra of SB galaxies, based on evolutionary populations of Galactic stars and adopting template X-ray spectra for the relevant emission processes. They suggested that high- and low-mass X-ray binaries (HMXBs, LMXBs) contribute most of the 2–15 keV spectrum, in the absence of AGN emission. Both categories of X-ray binaries have spectra that can be described as variously cut-off PLs (White, Swank & Holt 1983; Christian & Swank 1997). For example, in the case of one isolated episode of intense star formation, the 2–10 keV emission of the SB would be dominated by HMXBs, and would be described as a $\Gamma = 1.2$ power law. In more moderate SBs (such as those observed in local SB galaxies), in addition to the HMXBs related to the SB proper, also the LMXB population in the underlying disc is expected to provide important

[1] Various authors have analysed X-ray data on specific nearby starbursts: Ptak et al. (1997) and Cappi et al. (1999) for NGC 253 and M82; Okada, Mitsuda & Dotani (1997) for M83; Della Ceca et al. (1996) for NGC 1569; Della Ceca et al. (1999) for NGC 2146; Moran, Lehnert & Helfand (1999) for NGC 3256; Della Ceca, Griffiths & Heckman (1997) for NGC 4449; Zezas, Georgantopoulos & Ward (1998) and Della Ceca et al. (2002) for NGC 3310 and 3690 (Arp 299). See also Dahlem, Weaver & Heckman (1998) for a review.

contributions to the X-ray emission. In the case of a mix of HMXBs and LMXBs of various luminosities with Galactic proportions, the 2–10 keV emission can be described as a cut-off PL of the form $E^{-\Gamma}\,\mathrm{e}^{-E/kT}$, with photon index $\Gamma \sim 1.1$ and cut-off energy $kT \sim 8$ keV (Persic & Rephaeli 2002). This spectrum is to be corrected for the intrinsic absorption with variable column density $N_{\rm H}$.

5.3 Spectral decompositions

Following the above guidelines, we have tried to fit the spectra of our ULIRGs with various astrophysically motivated composites. The first clear feature to consider is the ubiquitous low-energy excess emission between 0.5 and 1 keV. One possibility to explain it would be a reflected component by photoionized gas, as found for example in the type 2 Seyfert galaxy NGC 1068 (Kinkhabwala et al. 2002; Brinkman et al. 2002). We have tried to reproduce the source spectra with such an emission, but in all cases have failed to obtain acceptable fits. In particular, for IRAS 19254−7245 the Fe K line at 6.49 keV detected by Braito et al. (2003a) implies the presence of an essentially cold neutral gas, which is unable to explain the low-energy emission features. For Mrk 231, Braito et al. (2003b) attempt to explain it entirely with an ionized reflection, which provides however a very poor overall fit, while a thermal ionized gas emission is required by the data. As for IRAS 20551−4250, an attempt to fit the low-energy spectrum with photoionized emission is similarly unsuccessful, as it would require an unphysically large value of the X-ray spectral index Γ and would generate a quite poor overall fit.

Also in the sources of all other samples the photoionized AGN emission model would leave significant residuals in all cases, which implies that collisionally ionized hot thermal gas is in any case required. We have modelled this ubiquitous low-energy thermal component with the Mekal/XSPEC code at constant (solar) metallicity (for the source IRAS 15250+3609 a two-temperature component was required). Then we have added a PL with photon index Γ, photoelectrically absorbed through a column density $N_{\rm H}$ to describe the hard X-ray excess that shows up at energies $\geqslant$2 keV. For IRAS 20551−4250 we have used the 'leaky-absorber' model (Section 4.3), while for Mrk 231 we have not considered in the present analysis the highly extinguished ($N_{\rm H} > 10^{24}$ cm^{-2}) component found in *BeppoSAX* data by Braito et al. (2003b). Alternatively, for all the sources we have attempted also to fit the high-energy data with an X-ray binary model with $\Gamma = 1.1$, cut-off energy $kT \sim 8$ keV and variable low-energy absorbing column density $N_{\rm H}$ (see Section 5.2).

The results of these spectral decompositions are reported in Table 4 and shown in Figs 4 and 5. In Fig. 6 we explore possible relationships between the best-fitting parameters. Fig. 6(a) is a plot of the ratio between the luminosities of the thermal and PL components (after correction for intrinsic absorption), as a function of the X-ray luminosity measured in the total 0.5–10 keV band. SB-dominated ULIRGs (starred symbols) occupy a fairly well-defined region with $L_{\rm total} \sim 10^{42}$ erg s^{-1} and $L_{\rm thermal}/L_{\rm PL} \gtrsim 0.2$. IRAS 12112+0305 appears to have a very low value of $L_{\rm thermal}$ compared with other SBs. The AGN-dominated sources have enhanced X-ray luminosities with $L_{\rm thermal}/L_{\rm PL} \leqslant 0.1$: as expected, these AGN ULIRGs have an energetically dominant power-law component. In the following we use the symbol $L_{\rm PL}$ to indicate the luminosity derived from the fit with a generic PL, rather than the one corresponding to the best-fitting X-ray binary model (in any case the difference between the two is a few tens per cent at most, see Table 4).

Table 4. Observed ULIRGs classification. Column (1): Object name. Column (2): Optical classification – liner (L), AGN or H II region (Lutz et al. 1999; Veilleux et al. 1999). Column (3): Mid-infrared classification based on *ISO* spectroscopy – starburst (SB) or AGN (Genzel et al. 1998). Column (4): X-ray classification.

(1) Name	(2) Optical	(3) Mid-IR	(4) X-ray
IRAS 12112+0305	L	SB	SB
Mrk 231	AGN-1	AGN	AGN
IRAS 14348−1447	L	SB	SB
IRAS 15250+3609	L	SB	SB
IRAS 17208−0014	H II	SB	SB
IRAS 19254−7245	AGN-2	SB	AGN
IRAS 20100−4156	H II	SB	SB/AGN
IRAS 20551−4250	H II	SB	AGN
IRAS 22491−1808	H II	SB	SB
IRAS 23128−5919	H II	SB	SB/AGN

Fig. 6(b) compares the luminosities of the thermal and PL components: a fairly clear correlation is apparent, with the AGN population occupying the high-luminosity end in both quantities. Again the AGN-dominated sources show an excess of the PL component luminosity compared with that of the thermal plasma.

Fig. 6(c) plots the luminosities of the thermal component $L_{\rm thermal}$ against the bolometric far-IR luminosities $L_{\rm FIR}$, while Fig. 6(d) does the same for the luminosities of the PL component. If we consider the SB-dominated population, both the $L_{\rm PL}$ and $L_{\rm FIR}$ luminosities appear reasonably correlated, while the AGN-dominated sources show similar $L_{\rm FIR}$ values but largely enhanced X-ray PL emission. On the contrary, we find a remarkable lack of correlation between $L_{\rm FIR}$ and the emissivity of the thermal component.

Finally, Fig. 6(e) shows that the SB-dominated sources have fairly well-defined $L_{\rm X}/L_{\rm FIR}$ ratios for both the thermal and PL components. The AGN sources display the usual excess of PL emission. In this regard, the sources IRAS 20100−4156 and 23128−5919 tend to occupy positions in the various plots that are intermediate between SB- and AGN-dominated populations, and may have genuinely intermediate properties.

6 DISCUSSION

Altogether, there are some remarkable regularities emerging from the spectral analysis of the *XMM–Newton* data.

The first one is that hot thermal plasma emission, likely a SB signature, is present in all objects of the sample. We find, however, a remarkable lack of correlation between thermal emission and far-IR luminosity (which is supposed to be a good indicator of the rate of star formation in the Galaxy). Our conclusion is that, although this plasma emission should be traced back to a Galactic wind triggered by young and exploding stars, the process may be ruled by various additional parameters, like the density and pressure of the surrounding ISM. According to the study by Strickland & Stevens (2000), the soft X-ray emission from SB-driven Galactic winds comes from a low filling factor ($\leqslant$2 per cent) gas, which contains only a small fraction ($\leqslant$10 per cent) of the mass and energy of the wind. Soft X-ray observations therefore do not probe the gas that contains the bulk of the energy, mass or metals in the outflow, while the bulk of the hot plasma radiates and cools on time-scales longer than that of the SB evolution.

To test the possible effect of the long cooling time, we have attempted to compare the thermal X-ray emissivity with the SB ages.

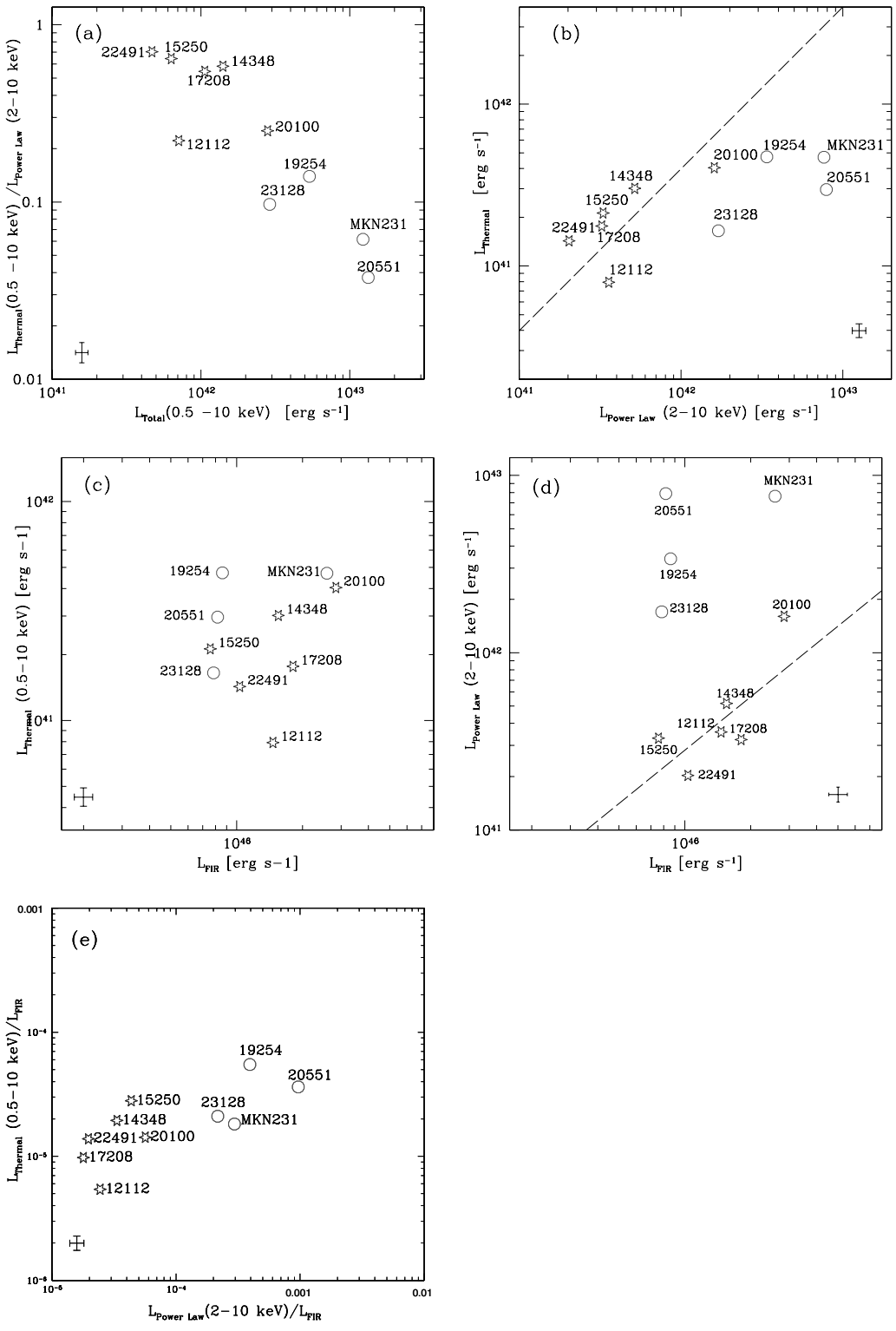

Figure 6. Luminosity–luminosity plots of various emission components identified in the *XMM–Newton* spectra of the ULIRG sample. Starred symbols refer to sources that we classify as dominated by starbursts, open circles to AGN-dominated sources. (a) Luminosity ratio between the thermal and the power-law (2–10 keV) components after correction for intrinsic absorption, versus the X-ray luminosity measured in the total 0.5–10 keV band. (b) Luminosity–luminosity plot of the thermal versus PL components. (c) and (d) Luminosities of the thermal and PL components against the bolometric far-IR luminosities $L_{\rm FIR}$. (e) The ratios of the thermal and PL luminosities to the bolometric far-IR luminosity $L_{\rm FIR}$. Dashed lines indicate proportionality relations.

To this end, since all optical counterparts of our sources show double or multiple nuclei (supposed in a merging system), we have adopted as a rough estimate of the merger stage the separation of the nuclear components, and investigated possible relations between the ratio of the thermal X-ray to IR luminosities against nuclear separation. We found essentially no correlations in these plots, which suggests that various parameters in addition to the star formation rate (SFR), like the pressure of the surrounding medium, should affect the thermal

plasma emission. In any case, the soft thermal emission is a quite poor tracer of the ongoing SFR.

On the contrary, the PL emission fitting the hard X-ray excesses in the spectra of our SB-dominated ULIRGs seems well correlated with $L_{\rm FIR}$. We understand this as an effect of both quantities being closely linked to the newly formed stellar populations, in one case ($L_{\rm FIR}$) due to dust reprocessing of the ultraviolet flux by young massive stars, in the other ($L_{\rm PL}$) due to the number of HMXBs which are a subset of the young stellar population (see below).

6.1 Stellar contribution to the X-ray emission

We now check the hypothesis that, in ULIRGs not dominated by an AGN, the hard X-ray 2–10 keV emission may be mainly due to luminous ($L_{2-10\,\rm keV} > 10^{37}$ erg s^{-1}) HMXBs. To this aim, we compare the star formation rate (SFR) estimated from the X-ray flux with that traced by the far-IR, under the assumption that both the X-ray emitting HMXBs and the OB stars heating the dust responsible for the far-IR flux are short-lived, in which case they can both be used as indicators of the ongoing SFR. Our definition of the SFR assumes a standard Salpeter stellar initial mass function (IMF) between 0.1 and 100 $\rm M_\odot$.

We proceed as follows. Assuming a mean HMXB luminosity of $L_{2-10\,\rm keV} = 5 \times 10^{37}$ erg s^{-1} (e.g. White et al. 1983), we first estimate the number of HMXBs from the 2–10 keV luminosity for each sample object. We consider that our Galaxy, hosting $\sim$50 bright HMXBs (Iben, Tutukov & Yungelson 1995, and references therein), has a SFR of $\sim$3 $\rm M_\odot$ yr^{-1} (e.g. Matteucci 2002). From the number of HMXBs we then estimate the corresponding $\rm SFR_{X-ray}$.

Then from the far-IR luminosity, we calculate (Kennicutt 1998)

$$\rm SFR_{FIR} \simeq L_{FIR}/(2.2 \times 10^{43}\,erg\,s^{-1})\,M_\odot\,yr^{-1}.$$

We plot the two independent estimates of the SFR in Fig. 7: this shows that the two are in quite good agreement for these non-AGN-dominated objects (filled circles), whereas the $\rm SFR_{X-ray}$ values are clearly in excess for the AGN-dominated sources (empty squares). Given the linear relation between SFR, far-IR and X-ray luminosities, this is obviously nothing other than the $L_{\rm FIR}$–$L_{2-10\,\rm keV}$ plot of Fig. 6(d), recast in different units.

We have further checked this X-ray to far-IR relationship on a sample of well-known moderate- to low-luminosity local SB galaxies, shown in Fig. 7 as crosses (see figure caption for references). While comparing these with ULIRGs, and following our previous discussion in Section 5.2, we bear in mind one relevant difference between the two classes: The star-forming activity in ULIRGs is very intense, short-lived and dominates the whole galaxy, so the hard X-ray flux is produced mainly by HMXBs. In lower SFR SB galaxies the X-ray flux is produced by a mix of HMXBs and LMXBs, coming respectively from SB regions and from the underlying quiescent disc, in comparable proportions. In Fig. 7 we have quantified this effect by the parameter f, the fraction of 2–10 keV emission attributable to HMXBs, setting $f = 1$ for ULIRGs and $f \simeq 0.25$ for SBs (Persic & Rephaeli 2002).

These results confirm that, for ULIRGs without dominant AGN components, the 2–10 keV flux from ULIRGs is a good SFR indicator:

$$\rm SFR_{X\text{-}ray}^{ULIRG} \simeq \frac{L_{2\text{–}10keV}}{(10^{39}\,erg\,s^{-1})}\,M_\odot\,yr^{-1} \qquad (1)$$

for $L_{2-10\,\rm keV} \geqslant 10^{41}$ erg s^{-1}. For lower-luminosity SB galaxies ($L_{2-10\,\rm keV} < 10^{41}$ erg s^{-1}), the relation of the X-ray flux to the SFR is less straightforward, as a result of the contribution of long-lived

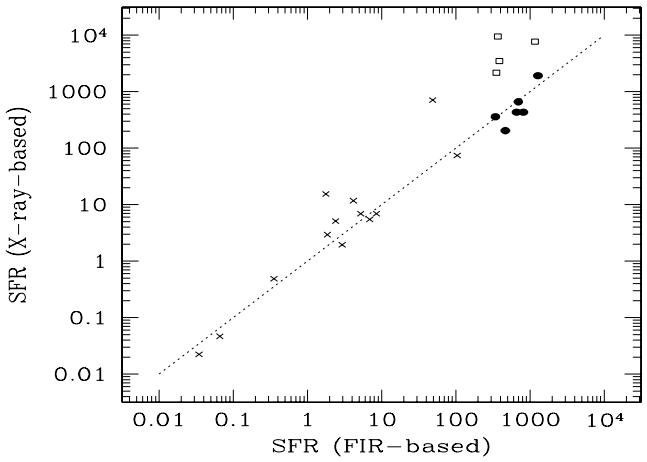

Figure 7. The SFR estimated from X-ray emission versus that estimated from far-IR emission. Empty squares and filled circles represent, respectively, AGN-dominated and non-AGN-dominated ULIRGs (from our sample), while crosses denote SB galaxies (from the literature). We used a representative SB sample (see Section 5.2), for which: (i) distances and far-IR luminosities come from Shapley, Fabbiano & Eskridge (2001) (M82, M83, NGC 253, 1569, 3079, 3310, 3628, 3690 and 4631), Dahlem et al. (1998) (NGC 55 and 4666), Della Ceca et al. (1999) (NGC 2146), and Moran et al. (1999) (NGC 3256); and (ii) 2–10 keV fluxes come from Dahlem et al. (1998) (M82, NGC 55, 253, 3079, 3628 and 4631), Okada et al. (1997) (M83), Della Ceca et al. (1996) (NGC 1569), Della Ceca et al. (1999) (NGC 2146), Moran et al. (1999) (NGC 3256), Zezas et al. (1998) (NGC 3310 and 3690), and Persic et al. (in preparation) (NGC 4666). The dotted line marks the relation $\rm SFR_{X-ray} = SFR_{FIR}$. The source with $\rm SFR_{X-ray} \simeq 750$ and $\rm SFR_{FIR} \simeq 50\ M_\odot\ yr^{-1}$ corresponds to NGC 3690 (Arp 299), which was found by Della Ceca et al. (2002) to contain an absorbed AGN.

LMXBs. In this case the relation becomes

$$\rm SFR_{X\text{-}ray}^{SB} \simeq \left(\frac{\mathit{f}}{0.25}\right) \frac{L_{2\text{–}10\,keV}}{(4 \times 10^{39} erg\,s^{-1})}\,M_\odot\,yr^{-1}. \qquad (2)$$

These results are in fair agreement with those found by Ranalli, Comastri & Setti (2002) and Gilfanov, Grimm & Sunyaev (2003), if we consider the different definitions of the SFR. Note that the only SB galaxy lying far outside the one-to-one relation in Fig. 7 is the crossed symbol with $\rm SFR_{X-ray} \sim 750\ M_\odot\ yr^{-1}$ corresponding to the galaxy Arp 299, which was recently proven to host a luminous obscured AGN (Della Ceca et al. 2002).

Finally, our *XMM–Newton* data below $\sim$0.5 keV have in all cases a very low S/N ratio, which does not allow us to constrain the origin of this part of the ULIRG spectrum. In some instances (IRAS 12112+0305 and 22491−1808) our formal fit implies a dominance of X-ray binary emission at such low energies, which may not be physical due to the fact that binary spectra typically show photoelectric absorption. To address this problem with more elaborate model spectra would need higher spectral resolution and S/N ratio data.

6.2 The AGN contribution to the ULIRG phenomenon

Altogether, we find in three of the 10 sample sources (Mrk 231, IRAS 19254−7245 and 20551−4250) various independent pieces of evidence for the presence of an absorbed AGN dominating the *XMM–Newton* X-ray spectrum. They show, in particular, values of the 2–10 keV luminosity (after absorption correction) quite in excess compared with the thermal plasma luminosities. This evidence is confirmed in all three objects by X-ray spectral features like a strong Fe K 6.4 keV line and a very flat or inverted hard X-ray spectrum

indicative of high column density ($N_{\rm H} > 10^{22}$ cm^{-2}) circumnuclear material.

The source IRAS 23128−5919 displays a hard spectrum and large X-ray luminosity that suggest an AGN contribution. Both IRAS 23128−5919 and 20100−4156 display intermediate values of the parameters in Fig. 6 between the AGN- and SB-dominated sources, which might indicate that an AGN contribution may be present.

It should be noticed that, among X-ray AGNs, IRAS 19254−7245, 20551−4250 and 23128−5919 did not show any AGN signatures from spectroscopy of IR coronal lines (Genzel et al. 1998). Consider however that, as shown in Fig. 6(e), the X-ray luminosity is only a tiny fraction (∼0.01 per cent and ∼0.1 per cent for SBs and AGNs, respectively) of the bolometric one. Then even for *bona fide* X-ray AGNs, the IR spectrum may well be dominated by the SB, hence explaining the results of the IR spectroscopy. Although the lack of AGN signatures in the IR spectra of these sources might alternatively be explained as dust obscuration up to 30 μm, the evidence for SB components in the X-ray spectra suggests that indeed an important fraction of the bolometric IR flux is likely to be of stellar origin (see previous Section and Fig. 7).

Though limited by the small statistics of our ULIRG sample, our conclusion is that for a majority of these sources the high rate of star formation indicated by the large far-IR luminosity can account for most of the X-ray emission. The X-ray spectra of roughly half of the ULIRGs show evidence of AGN contributions on top of an, always present, SB component. These results appear consistent with those based on a *Chandra* survey by Ptak et al. (2003).

7 CONCLUSION

We have devoted a large observing programme with *XMM–Newton* to survey the hard X-ray properties of a complete and representative sample of ultraluminous IR galaxies, as a way to probe deeply into the heavily extinguished cores of this still physically elusive class of sources. All the 10 observed ULIRGs have been detected with high statistical significance by *XMM–Newton*, but their 2–10 keV fluxes turned out to be rather faint on average.

The X-ray emission appears to be extended on a scale of ∼30 kpc for Mrk 231 and IRAS 19254−7245, possibly evidence of Galactic superwinds. In these same sources, IRAS 20551−4250 and 23128−5919, we find evidence for the presence of hidden AGNs, while a minor AGN contribution may be suspected also in IRAS 20100−4156. A strong Fe K line (EW ∼ 2 keV) in the X-ray spectrum of IRAS 19254−7245 and a much weaker line in Mrk 231 (EW ∼ 0.2 keV) are also detected, suggestive of deeply buried type II quasars (Braito et al. 2003a,b). For the other sources, hence for roughly half of the ULIRG sample, the X-ray luminosities and spectral shapes are mostly consistent with hot thermal plasma and X-ray binary emissions of mainly starburst origin.

We have analysed the *XMM–Newton* spectra in terms of various physical components, that is, thermal plasma emission and hard X-ray power laws due to either X-ray binaries or true AGNs. We have found interesting regularities in the source parameters. Thermal plasma emission, the signature of a starburst component and dominating the spectra between 0.5 and 1 keV, is present in all the sample objects. The alternative interpretation of this soft X-ray component as due to a reflected emission by AGN-photoionized gas is mostly excluded by our analysis.

This thermal emission is quite unrelated with the far-IR luminosity (a tracer of the ongoing star formation rate), from which we infer that other parameters should determine it in addition to the rate of star formation. On the contrary, the X-ray binary power-law emission fitting the hard X-ray component in the starburst-dominated ULIRGs is correlated with $L_{\rm FIR}$, both quantities tracing the number of young stars in the galaxy and measuring the ongoing SFR.

We fully confirm with these data the composite nature of ULIRGs as a class, with indications for a predominance of the starburst over the AGN phenomenon even when observed in hard X-rays.

ACKNOWLEDGMENTS

The work reported herein is based on observations obtained with *XMM–Newton*, an ESA science mission with instruments and contributions funded by ESA Member States and the USA (NASA).

We thank the referee, Dr K. Iwasawa, for his careful reading of the paper and very useful comments. This work received financial support from ASI (I/R/037/01 and I/R/062/02) under the project 'Cosmologia Osservativa con *XMM–Newton*' and support from the Italian Ministry of University and Scientific and Technological Research (MURST) through grants Cofin 00–02–004. PS acknowledges financial support by the Italian Consorzio Nazionale per l'Astronomia e l'Astrofisica (CNAA).

REFERENCES

Berta S., Fritz J., Franceschini A., Bressan A., Pernechele C., 2003, A&A, 403, 119
Braito V. et al., 2003a, A&A, 398, 107
Braito V. et al., 2003b, A&A, submitted
Brandt W. N., Fabian A. C., Takahashi K., Fujimoto R., Yamashita A., Inoue H., Ogasaka Y., 1997, MNRAS, 290, 617
Brinkman A. C., Kaastra J. S., van der Meer R. L. J., Kinkhabwala A., Behar E., Kahn S. M., Paerels F. B. S., Sako M., 2002, A&A, 396, 761
Cappi M. et al., 1999, A&A, 350, 777
Charmandaris V. et al., 2002, A&A, 391, 429
Christian D. J., Swank J. H., 1997, ApJS, 109, 177
Dahlem M., Weaver K. A., Heckman T. M., 1998, ApJS, 118, 401
David L. P., Jones C., Forman W., 1992, ApJ, 388, 82
Della Ceca R., Griffiths R. E., Heckman T. M., MacKenty J. W., 1996, ApJ, 469, 662
Della Ceca R., Griffiths R. E., Heckman T. M., 1997, ApJ, 485, 581
Della Ceca R., Griffiths R. E., Heckman T. M., Lehnert M. D., Weaver K. A., 1999, ApJ, 514, 772
Della Ceca R. et al., 2002, ApJ, 581, L9
Devereux N. A., Young J. S., 1989, ApJ, 371, 515
Ehle M. et al., 2001, The XMM–Newton Users' Handbook: Issue 2.1 (http://xmm.gsfc.nasa.gov/docs/xmm/uhb/xmm_uhb.html)
Elbaz D., Cesarsky C. J., Chanial P., Aussel H., Franceschini A., Fadda D., Chary R. R., 2002, A&A, 384, 848
Franceschini A., Mazzei P., De Zotti G., Danese L., 1994, ApJ, 427, 140
Franceschini A., Aussel H., Cesarsky C., Elbaz D., Fadda D., 2001, A&A, 378, 1
Gallagher S. C., Brandt W. N., Chartas G., Garmire G. P., Sambruna R. M., 2002, ApJ, 569, 655
Genzel R., Cesarsky C. J., 2000, ARA&A, 38, 761
Genzel R. et al., 1998, ApJ, 498, 579
Gilfanov M., Grimm H. J., Sunyaev R., 2003, MNRAS, submitted (astro-ph/0301331)
Hauser M. G. et al., 1998, ApJ, 508, 25
Iben I., Jr, Tutukov A. V., Yungelson L. R., 1995, ApJS, 100, 217
Imanishi M., Ueno S., 1999, ApJ, 527, 709
Imanishi M., Dudley C. C., Maloney P. R., 2001, ApJ, 558, L93
Iwasawa K., 1999, MNRAS, 302, 96
Kennicutt R. C., Jr, 1998, ApJ, 498, 541
Kinkhabwala A. et al., 2002, ApJ, 575, 732
Lagache G., Haffner L. M., Reynolds R. J., Tufte S. L., 2000, A&A, 354, 247

Lilly S. J., Eales S. A., Gear W. K. P., Hammer F., Le Fèvre O., Crampton D., Bond J. R., Dunne L., 1999, ApJ, 518, 641
Lutz D. et al., 1996, A&A, 315, L137
Lutz D., Veilleux S., Genzel R., 1999, ApJ, 517, L13
Maloney P. R., Reynolds C. S., 2000, ApJ, 545, L23
Matteucci F., 2002, Proc. XIII Canary Islands Winter School Astrophys., Cosmochemistry: The Melting Pot of Elements, in press (astro-ph/0203340)
Melnick J., Mirabel I. F., 1990, A&A, 231, 19
Mewe R., Gronenschild E. H. B. M., van den Oord G. H. J., 1985, A&AS, 62, 197
Misaki K. et al., 1999, in Cohen R. J., Sullivan W. T., Proc. IAU Symp. 196, Preserving the Astronomical Sky: an IAU/COSPAR/UN Special Environmental Symposium, Astron. Soc. Pac., San Francisco, p. 360
Mizuno T., Ohbayashi H., Iyomoto N., Makishima K., 1998, in Koyama K., Kitamoto S., Itoh M., eds, Proc. IAU Symp. 188, The Hot Universe. Kluwer, Dordrecht, p. 284
Moran E. C., Lehnert M. D., Helfand D. J., 1999, ApJ, 526, 649
Okada K., Mitsuda K., Dotani T., 1997, PASJ, 49, 653
Pappa A., Georgantopoulos I., Stewart G. C., 2000, MNRAS, 314, 589
Persic M., Rephaeli Y., 2002, A&A, 382, 843
Ptak A., Serlemitsos P. J., Yaqoob T., Mushotzky R., Tsuru T., 1997, AJ, 113, 1286
Ptak A., Heckman T., Levenson N. A., Weaver K., Strickland D., 2003, ApJ, in press (astro-ph/0304222)
Ranalli P., Comastri A., Setti G., 2002, in Jansen F. et al., eds, ESA-SP488, New Visions of the X-Ray Universe in the XMM–Newton and Chandra Era. ESA Publications Division, Noordwijk, in press (astro-ph/0202241)
Rigopoulou D., Spoon H. W. W., Genzel R., Lutz D., Moorwood A. F. M., Tran Q. D., 1999, AJ, 118, 2625
Risaliti G., Gilli R., Maiolino R., Salvati M., 2000, A&A, 357, 13
Sanders D. B., Mirabel F., 1996, ARA&A, 34, 749
Sanders D. B., Soifer B. T., Elias J. H., Madore B. F., Matthews K., Neugebauer G., Scoville N. Z., 1988, ApJ, 325, 74
Shapley A., Fabbiano G., Eskridge P. B., 2001, ApJS, 137, 139
Smail I., Ivison R., Blain A. W., 1997, ApJ, 490, L5
Smail I., Ivison R. J., Blain A. W., Kneib J.-P., 2002, MNRAS, 331, 495
Smith P. S., Schmidt G. D., Allen R. G., Angel J. R. P., 1995, ApJ, 444, 146
Soifer B. T. et al., 1984, ApJ, 278, L71
Soifer B. T., Sanders D. B., Madore B. F., Neugebauer G., Danielson G. E., Elias J. H., Lonsdale C. J., Rice W. L., 1987, ApJ, 320, 238
Soifer B. T. et al., 2001, AJ, 122, 1213
Strickland D. K., Stevens I. R., 2000, MNRAS, 314, 511
Strickland D. K., Heckman T. M., Weaver K. A., Dahlem M., 2000, AJ, 120, 2965
Strüder L. et al., 2001, A&A, 365, L18
Turner M. J. L. et al., 2001, A&A, 365, L27
Turner T. J., 1999, ApJ, 511, 142
Veilleux S., Sanders D. B., Kim D.-C., 1997, ApJ, 484, 92
Veilleux S., Kim D.-C., Sanders D. B., 1999, ApJ, 522, 139
Vignati P. et al., 1999, A&A, 349, 57
White N. E., Swank J. H., Holt S. S., 1983, ApJ, 270, 711
Zezas A. L., Georgantopoulos I., Ward M. J., 1998, MNRAS, 301, 915

This paper has been typeset from a TEX/LATEX file prepared by the author.